Catalysis Science & Technology

Pt1-O4 as active sites boosting CO oxidation via a non-classical MvK mechanism

Journal:	*Catalysis Science & Technology*
Manuscript ID	CY-ART-01-2021-000115.R1
Article Type:	Paper
Date Submitted by the Author:	16-Mar-2021
Complete List of Authors:	Lou, Yang; Jiangnan University, School of Chemical and Materials Engineering Zheng, Yongping; Shenzhen Institutes of Advanced Technology Chinese Academy of Sciences, Guo, Wenyi; Jiangnan University Liu, Jingyue; Arizona State University, Department of Physics

Pt_1-O_4 as active sites boosting CO oxidation via a non-classical MvK mechanism

Yang Lou[1,2,*], Yongping Zheng[3,*], Wenyi Guo[2], Jingyue Liu[1,*]

[1]*Department of Physics, Arizona State University, Tempe, Arizona 85287, United States*

[2]*International Joint Research Center for Photoresponsive Molecules and Materials, Key Laboratory of Synthetic and Biological Colloids, Ministry of Education, School of Chemical and Material Engineering, Jiangnan University, Wuxi, Jiangsu 214122, China*

[3]*Functional Thin Films Research Center, Shenzhen Institutes of Advanced Technology, Chinese Academy of Sciences, Shenzhen, 518055, China*

[*]*Corresponding author: yang.lou@jiangnan.edu.cn; yp.zheng@siat.ac.cn; jingyue.liu@asu.edu.*

Abstract:

Single-atom catalysts (SACs) possess excellent performance for various catalytic reactions but it is still challenging to have adequate total activity for practical applications. Here we report the high-valence, square planar Pt_1-O_4 as an active site enables to significantly increase the total activity of Pt_1/Fe_2O_3 SAC with a Pt loading of only ~30 ppm, which is similar to that of a 1.0 wt.% nano-Pt/Fe_2O_3 for CO oxidation at 350 ^oC. Density functional theory calculations reveal the Pt_1-O_4 catalyzes CO oxidation through a non-classical Mars–van Krevelen mechanism. The adsorbed O_2 on Pt_1 atoms activates the coordination oxygen in Pt_1-O_4 configuration and then a barrierless O_2 dissociation occurs on the Pt_1-Fe_2 triangle to replenish the consumed coordination oxygen by the cooperative action of Pt 5*d* and Fe 3*d* electrons. This work provides a new fundamental understanding of oxidation catalysis on stable and active SACs, providing guidance for rationally designing future heterogeneous catalysts.

Keywords: ***Single-atom catalyst; Reducible metal oxide; CO oxidation; Reaction mechanism; Super active catalyst.***

1. Introduction

Noble metal-based catalysts have been widely utilized in various important chemical transformations.[1-3] However, most of the noble metal-based catalysts have low atom efficiency since their dispersion is much less than 100%, especially for larger nanoparticles (NPs), which significantly increases the usage of noble metal and unavoidably increases the cost of supported noble metal catalysts. The recently developed single-atom catalysts (SACs) have the potential of increasing the atom efficiency to 100% and thus significantly decreases the cost of supported noble metal catalysts[4-8], which also demonstrate excellent performance for various important catalytic reactions.[9-19] However, the major issues for practical applications of SACs are the low total activity (defined as the catalytic activity based on the total weight of the catalyst including both the active metal component and the support) due to the low levels of metal loading and, in some cases, the sintering during catalytic reactions, especially at high reaction temperatures.[20-23] Progress toward stabilizing single metal atoms and significantly increasing the total activity of SACs is critical to advancing SACs for commercial applications. One approach to solve this problem is to anchor high-number-density single metal atoms on the support surfaces so that the total activity of the synthesized SACs can be significantly increased.[11] Another approach is to make each catalytic site super active so that even with low levels of isolated metal atoms, the total activity of the fabricated SACs is high enough for practical applications.

The term of highly active catalysts has been defined based on the activity of supported Au catalysts for CO oxidation[24], which corresponds to 20 $mmol_{CO}$ g_{cat}^{-1} h^{-1} for a 1 wt.% Au loading. Although the specific reaction rate (calculated on the basis of active metal species) of single metal atoms may be higher than that of their NP counterparts, the total activity of a stable SAC can barely satisfy the definition of highly active catalysts due to the low-number-density of the active metal atoms. When the catalytic activity of each single metal atom is significantly increased the total catalytic activity of a SAC can be comparable to their NP counterparts which usually require high levels of metal loading. We define such SACs as super active, in analogy to super active Ziegler-Natta catalysts used in polymer synthesis such as olefin polymerization.[25-28] These super active polymerization catalysts have achieved important production process innovations[29], which have influenced our daily life in countless beneficial ways.

In this work, we report that by constructing a unique Pt_1-O_4 structural configuration as the active site, single Pt (Pt_1) atoms supported on reducible metal oxides (e.g., Fe_2O_3 and CeO_2)

can become super active for CO oxidation at elevated temperatures. For CO oxidation at 350 ^{o}C, the specific activity of the Pt_1/Fe_2O_3 SAC with a Pt loading of only ~30 ppm is similar to that of the nano-Pt/Fe_2O_3 catalyst with a Pt loading of ~ 1.0 wt.%. To our knowledge, this is the first time to report such super active behavior of a SAC under relatively high temperature reaction conditions. Density functional theory (DFT) calculations reveal that the high-valence Pt_1-O_4 active site efficiently catalyze CO oxidation through a non-classical Mars–van Krevelen (MvK) reaction pathway.

2. Experimental Section

2.1 Catalyst Preparation

The Fe_2O_3 and CeO_2 nanocrystallites are synthesized by a precipitation method. The iron (III) nitrate nonahydrate ($Fe(NO_3)_3{\cdot}9H_2O$, Sigma-Aldrich) and sodium carbonate (Na_2CO_3, Sigma-Aldrich) are used as precursor salt and precipitant. The obtained precipitates are dried at 60 ^{o}C for 12 h in air. The Fe_2O_3 and CeO_2 precipitates are calcined at 350 °C for 4 h and 400 °C for 5 h in air, respectively. The γ-Al_2O_3 is purchased from Inframat Advanced Materials.

Single Pt atoms are dispersed onto the surfaces of Fe_2O_3, CeO_2 and γ-Al_2O_3 by a strong adsorption method.[13, 14, 30] The corresponding amount of Pt ($H_2PtCl_4{\cdot}6H_2O$, Sigma-Aldrich) is firstly dispersed onto the Fe_2O_3, γ-Al_2O_3, and CeO_2 surfaces. The pH values of the Pt-containing solutions are finely controlled for each support material. Typically, pH value of 2.3 is used for Fe_2O_3 and 3.0 is used for γ-Al_2O_3 and CeO_2. After being aged at room temperature for 2 hours and filtered, the solid powders are dried at 60 °C for 12 h in air. The Pt/Fe_2O_3, Pt/γ-Al_2O_3, and Pt/CeO_2 catalysts are calcined at 300 °C for 2 h in air. The actual loadings of Pt measured by ICP-MS (Inductively Coupled Plasma Mass Spectrometry), on the Fe_2O_3, γ-Al_2O_3, and CeO_2 are 0.029 wt.%, 0.034 wt.%, and 0.013 wt.%, respectively.

The corresponding amount of Pd ($PdCl_2$, Sigma-Aldrich) is firstly deposited onto the surfaces of Fe_2O_3. The pH of the Pd-containing solutions is finely tuned to 3.8. After being aged at room temperature for 2 hours and filtered, the Pd/Fe_2O_3 powders are dried at (60 °C/12 h) and calcined at 300 °C for 2 h in air. The Pd actual loading on Fe_2O_3 is 0.17 wt.% measured by ICP-MS.

Pt particles over Fe_2O_3 and CeO_2 are synthesized by a colloid method[5]. Typically, NaOH

(2.32 mmol) and $H_2PtCl_6 \cdot 6H_2O$ (5.16 μmol) is added into 13.3 ml glycol solution with stirring for 1 h at room temperature and then the resulting solution is heated at 140°C for 4 h to obtain the brown colloidal solution. Then 100 mg Fe_2O_3 (CeO_2) is dispersed in the obtained colloidal solution under stirring at room temperature. After stirring for 2 h, the precipitate is filtered and washed thoroughly by distilled water until free of chloride ions (tested by saturated $AgNO_3$ solution). The obtained precipitate is dried at (60 °C/12 h) and calcined at 350 °C for 4 h in air. The thorough DI washing and the air calcination processes assure that the organic residues on the Pt surfaces are eliminated.

The synthesized SACs are denoted as Pd_1/Fe_2O_3, Pt_1/Fe_2O_3, and $Pt_1/\gamma\text{-}Al_2O_3$ and the catalysts of Pt nanoparticles supported on Fe_2O_3 and CeO_2 are denoted as nano-Pt/Fe_2O_3 and nano-Pt/CeO_2, respectively.

2.2 Catalyst Characterization

The loadings of Pt species are measured by ThermoFinnegan iCAP Q quadrupole ICP-MS with CCT (Collision Cell Technology), which are run with a discrimination mode in kinetic energy by taking in-line aspiration as internal standard of multiple elements.

HAADF-STEM images are acquired on a JEM-ARM200F TEM/STEM with a resolution of 0.08 nm. Before collecting data, the catalysts are dispersed by ultrasonic machine in ethanol. Then a droplet of dispersed catalyst solution is dropped onto a copper grid coated with lacey carbon film. Low magnification images have been extensively screened to make sure that Pt nanoparticles are not present in the as-synthesized or used SACs. Atomic resolution images are used to screen the presence of individual Pt atoms and the absence of Pt clusters in both the fresh and used SACs.

Diffuse Reflectance Infrared Fourier Transform Spectroscopy (DRIFTs) of CO adsorption on Pt_1 and nano-Pt catalysts is conducted on FT-IR spectrometer (Nicolet 6700) with a MCT detector (cooled by liquid nitrogen). TheCaF_2 windows are equipped on sample cell. The DRIFTs are acquired with a resolution of 4 cm^{-1} and 64 scans in Kubelka-Munk units. When collecting the data of CO-DRIFTs on Pt_1 and nano-Pt, the samples are firstly heated at 120 ^oC for 40 min to remove the possible H_2O and other impurities on the surface. Then the samples

are cooled down to 25 ^{o}C and 50 ^{o}C respectively, and the background is acquired until the background is stable. Then CO (1 vol.% CO/He) molecules are allowed to adsorb on the catalyst surfaces until the adsorption of gaseous CO is saturated on the catalyst surfaces (~15 min). Then pure He is used to purge out the gaseous CO from the sample cell so that the chemically adsorbed/bound CO species can be observed. After collecting the background signal, the whole procedure was recorded by FTIR including the processes of CO adsorption and He purging.

The X-ray absorption fine structure spectra of the Pt_1/Fe_2O_3 SAC, nano-Pt/ Fe_2O_3, Pt_1/CeO_2 SAC, nano-Pt/CeO_2 and Pt foil experiments are collected at the Advanced Photon Source (APS) on beamline 10-BM (MRCAT) with electron energy 7 GeV with average current of 100 mA. The XAFS spectra are collected in fluorescence mode. Data reduction, data analysis, and EXAFS fitting are performed with the Athena and Artemis software packages. The energy calibration of the catalysts is conducted through a standard Pt foil and PtO_2.

2. 3 Kinetic Measurements

The specific reaction rate (calculated based on equation (1)) of all the synthesized nano-Pt/Fe_2O_3, Pt_1/Fe_2O_3 SAC, Pt_1/γ-Al_2O_3 SAC, Pd_1/Fe_2O_3 SAC and the corresponding supports (Fe_2O_3, and γ-Al_2O_3) is measured under a typical reaction condition of 1.0 vol.% CO, 4.0 vol.% O_2 and He balance. Feed gas compositions of 2.5 vol.% CO, 2.5 vol.% O_2 and He balance and 2.5 vol.% CO, 1.25 vol.% O_2 and He balance are also used for measuring the specific reaction rate of Fe_2O_3, nano-Pt/Fe_2O_3 and Pt_1/Fe_2O_3 SAC as well as the CeO_2, nano-Pt/CeO_2 and Pt_1/CeO_2 SAC catalysts. To eliminate the internal and external diffusion effects, the CO conversion rates are adjusted to below 20% when conducting the kinetic measurements by adjusting the hourly gas space velocity to calculate the reaction rates. The concentrations of CO and CO_2 in the outlet stream are measured by an on-line gas chromatograph (Agilent 7890A equipped with thermal conductivity detector).

Since the three different supports also possess catalytic activity for CO oxidation at elevated temperatures, we subtract the contribution of the support surfaces when we compare the catalytic behavior of the Pt_1 atoms supported on different supports and the supports are

treated following the same procedures as did on catalysts. Since the Pt loading is extremely low we can assume that the reaction rates originate from the Pt_1 atoms by subtracting the reaction rates of the supports from the reaction rates of the corresponding SACs. This treatment is justifiable as long as the total number of the supported Pt_1 atoms is much less than the total number of the surface atoms of the support material and that the activity of the SACs is much higher than that of the support.

The TOF is defined, in this case, as the amount of CO molecules converted over one Pt atom in one second and calculated based on equation (2).

$$r = \frac{C_{CO} \cdot X_{CO} \cdot V \cdot P_{atm}}{m_{cat} \cdot R \cdot T} (mol \cdot s^{-1} \cdot g_{cat}^{-1}) \quad (1)$$

$$TOF = \frac{(r_{catalyst} - r_{support}) \cdot N_A}{N_{Pt}} (s^{-1}) \quad (2)$$

Where the $r_{catalyst}$ and $r_{support}$ are reaction rates of catalysts and supports, respectively; m_{cat}: mass of catalyst in the reactor bed (g); C_{CO}: concentration of CO in the feed gas; V: total flow rate of the inlet gas mixture (m^3/s); X_{CO}: conversion rate of CO; R: molar gas constant (8.314 Pa • m^3 • mol^{-1} • K^{-1}); T: reaction temperature (K); P_{atm}: atmospheric pressure (101.3 KPa); N_A: Avogadro constant (6.02×10^{23} mol^{-1}); and N_{Pt}: the number of Pt atoms per gram of catalyst.

2. 4 DFT Calculation Methods

Computational studies are performed through spin-polarized density functional theory with Hubbard-U correction (DFT+U) (U_{eff} = 5 eV)[31] implemented in the Vienna *ab-initio* Simulation Package (VASP).[32] The generalized gradient approximation with the Perdew-Burke-Ernzerhof functional (PBE-GGA)[33] is adopted for the exchange correlation interactions. The projector augmented wave (PAW)[34] method and the plane-wave basis with an energy cutoff of 450 eV are used for efficient electronic calculations. The pseudopotential valence-electron configurations used in the calculations are Pt $5d^9 6s^1$, Fe $3d^6 4s^2$, O $2s^2 2p^4$, and C $2s^2 2p^2$. The structural calculations are relaxed to a force convergence of 0.01 eV·$Å^{-1}$ for each ionic step and an energy convergence of 10^{-5} eV for each electronic step. The *k*-space sampling is done using the Monkhorst-Pack grid with a *k* spacing less than 0.03 $Å^{-1}$. To get more reliable

free energies, the spin ordering of the simulated hematite α-Fe_2O_3 is considered and relaxed in its most preferable experimental antiferromagnetic configuration, i.e., spin-up and down Fe ions are antiferromagnetically aligned along the [001] direction and ferromagnetically ordered in each (001) FeO plane. This magnetic ordering is preserved in the slab calculation for the modeling of (001) surface. Additionally, the top and bottom surfaces in the slab supercell are spaced to more than 10 Å distance in vacuum to prevent any periodic image interaction. The over-binding energies of DFT-PBE calculated O_2, CO and CO_2 are corrected according to the previous reports.[31]

3. Results and Discussions

3. 1 Synthesis and Identification of Pt_1 SACs

Pt_1 atoms were dispersed onto the surfaces of Fe_2O_3 and CeO_2 nanocrystallites with a loading level of 0.029 wt.% and 0.013 wt.%, respectively, determined by the inductively coupled plasma mass spectrometry (ICP-MS) technique. By examining numerous low- and high- magnification HAADF-STEM images of both the fresh and used Pt_1/Fe_2O_3 SACs (Figure 1a-b and Figure S1-2) and Pt_1/CeO_2 SACs (Figure 1 c-d and Figure S3-4), we concluded that the as-synthesized and used Pt_1/Fe_2O_3 and Pt_1/CeO_2 SACs contained no Pt clusters/particles but only isolated Pt_1 atoms.

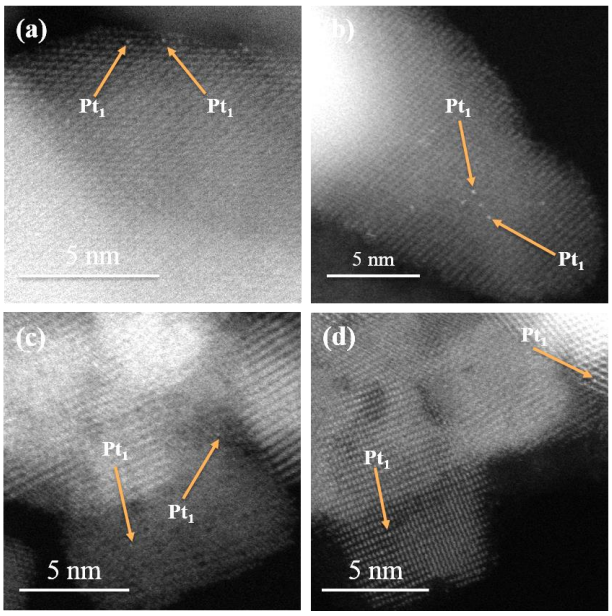

Figure 1 Atomic resolution HAADF-STEM images of used (a) and fresh (b) Pt_1/Fe_2O_3 SAC, and used (c) and fresh (d) Pt_1/CeO_2 SAC, clearly revealing the Pt_1 atoms in both the fresh and used SACs.

3. 2 Super Active behaviors of Pt_1 SAC for CO oxidation

Our experimental results show that the specific reaction rate of Pt_1 atoms supported on reducible metal oxides (Fe_2O_3 and CeO_2) for CO oxidation dramatically increased when the reaction temperature is higher than 260 °C (Figure 2). The Pt_1/Fe_2O_3 and Pt_1/CeO_2 SACs became super active for CO oxidation at temperatures around 350 °C with a specific reaction rate as high as 7.34 $mol_{CO} \cdot g_{Pt} \cdot s$ (1432.7 CO molecules per Pt atom per s) and 3.91 $mol_{CO} \cdot g_{Pt} \cdot s$ (762.1 CO molecules per Pt atom per s) with a feed gas mixture of 1.0 vol.% CO, 4.0 vol.% O_2 and He balance. After the CO oxidation reaction at 350 °C, the Pt_1 atoms were still in the form of isolated single atoms (Figure 1a and 1c), suggesting that the Pt_1 atoms did not sinter during the relatively high temperature CO oxidation process. More aberration-corrected HAADF-STEM images of the used Pt_1/Fe_2O_3 and Pt_1/CeO_2 SACs are displayed in Figure S2 and Figure S4, respectively, showing the presence of only Pt_1 atoms without any Pt clusters or NPs.

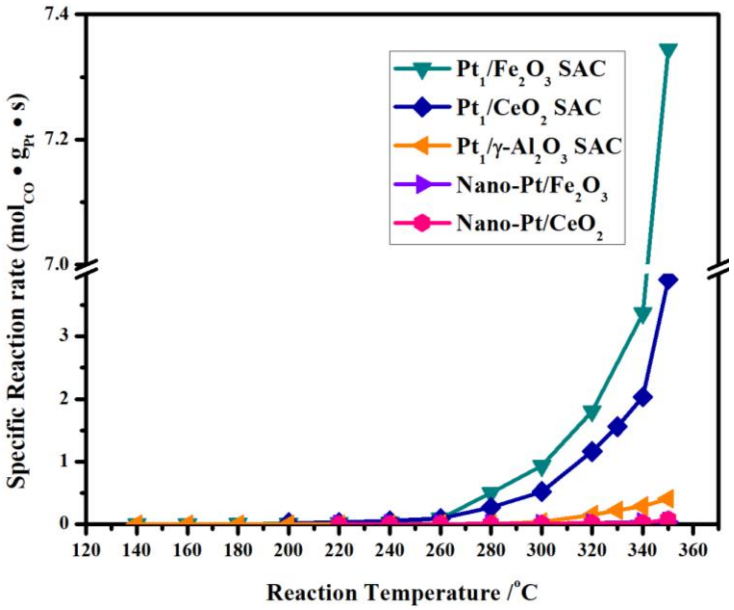

Figure 2 The specific reaction rate (per gram of Pt) for CO oxidation vs reaction temperature over Pt_1/Fe_2O_3 SAC, Pt_1/CeO_2 SAC, Pt_1/γ-Al_2O_3 SAC, nano-Pt/CeO_2 and nano-Pt/Fe_2O_3. Feed gas composition: 1 vol.% CO, 4 vol.% O_2 and He balance; space velocity: 9,000 l/g•h ~ 45,000 l/g•h; and Pressure: 0.1 MPa.

Fe_2O_3 supported Pt NPs (denoted as nano-Pt/Fe_2O_3) and CeO_2 supported Pt NPs (denoted as nano-Pt/CeO_2) with 0.62 wt.% Pt and 0.55 wt.% Pt (determined by ICP-MS), respectively, were synthesized by a colloidal method reported in literature[35] as reference samples. By analyzing numerous low- and high-magnification HAADF-STEM images of the nano-Pt/Fe_2O_3 (Figure S5) and nano-Pt/CeO_2 (Figure S6) catalysts, we concluded that the Pt NPs are uniformly distributed on the Fe_2O_3 and CeO_2 powders with an average size of 1.3 ± 0.1 nm and 4.0 ± 0.1 nm, respectively. The colloidal Pt NPs are thoroughly washed and calcined to assure the elimination of organic residues on the synthesized catalysts. Although the majority of the

Pt species were in the form of nanometer-sized particles, Pt_1 atoms were still detected (Figure S5 (b-d) and Figure S6 (d-e)) in these catalysts.

The specific reaction rates (per gram of Pt) at 350 °C under the same reaction conditions were estimated to be 0.04 $mol_{CO} \cdot g_{Pt} \cdot s$ and 0.08 $mol_{CO} \cdot g_{Pt} \cdot s$ over the nano-Pt/Fe_2O_3 and nano-Pt/CeO_2, which are ~190 and ~50 times lower than that on the Pt_1/Fe_2O_3 SAC and Pt_1/CeO_2 SAC, respectively. These catalytic evaluation results suggest that compared to reducible metal oxide Fe_2O_3 and CeO_2 supported Pt NPs the supported Pt_1 atoms are super active for CO oxidation at elevated temperatures (260 ^oC to 350 ^oC).

To demonstrate the importance of the metal oxide supports in facilitating the super activity of supported Pt_1 atoms, we further tested the performance of Pt_1 atoms supported on irreducible γ-Al_2O_3 support. The CO oxidation activity over the as-synthesized Pt_1/γ-Al_2O_3 SAC (HAADF-STEM images of fresh and used Pt_1/γ-Al_2O_3 SAC are shown in Figure S7 and Figure S8, respectively) is much lower with a specific reaction rate of only 0.41 $mol_{CO} \cdot g_{Pt} \cdot s$ at 350 ^oC (feed gas of 1.0 vol.% CO, 4.0 vol.% O_2 and He balance). These comparative studies unambiguously demonstrate that the Pt_1/Fe_2O_3 and Pt_1/CeO_2 SACs are super active for CO oxidation at elevated temperatures and that the reducible metal oxide support plays a major role in controlling the super active property of the Pt_1 atoms at elevated temperatures.

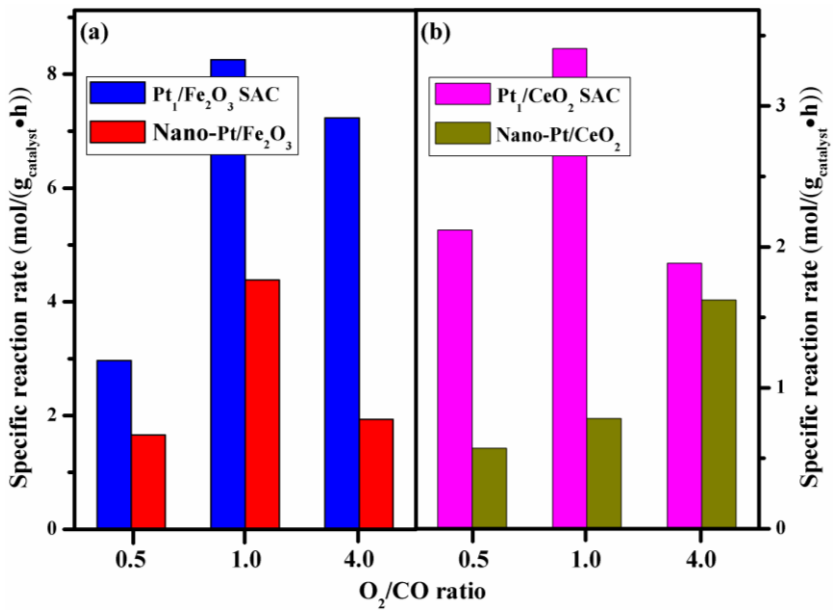

Figure 3 The total specific rate (per gram of catalyst) of the Pt_1/Fe_2O_3 SAC and nano-Pt/Fe_2O_3 (a) and Pt_1/CeO_2 SAC and nano-Pt/CeO_2 (b) catalysts for CO oxidation at 350 ^{o}C with different O_2/CO ratios. Three different feed gas compositions were used to measure the total specific rate of Pt_1 SACs and Pt nanoparticle catalysts for CO oxidation at 350 ^oC: 1) 1.0 vol.% CO, 4.0 vol.% O_2 and He balance (O_2/CO = 4.0); 2) 2.5 vol.% CO, 2.5 vol.% O_2 and He balance (O_2/CO = 1.0); and 3) 2.5 vol.% CO, 1.25 vol.% O_2 and He balance (O_2/CO = 0.5). The space velocity varied from 17,400 l/g•h to 45,000 l/g•h with pressure = 0.1M Pa.

We further evaluated the effect of the O_2/CO ratio on the total activity of the Pt_1/Fe_2O_3 and Pt_1/CeO_2 SACs at the temperatures that these SACs yield super active properties (Figure 3). The total activity of the Pt_1/Fe_2O_3 and Pt_1/CeO_2 SAC was as high as 8.26 $mol_{CO}/g_{catalyst}$·h and 3.41 $mol_{CO}/g_{catalyst}$·h, respectively, at 350 °C when the O_2/CO volume ratio is adjusted to ~1 (feed gas of 2.5 vol.% CO, 2.5 vol.% O_2 and He balance). When the O_2/CO ratio is increased to 4 (1.0 vol.% CO, 4.0 vol.% O_2 and He balance) or decreased to 0.5 (2.5 vol.% CO, 1.25 vol.% O_2 and He balance), the total activity changed to 7.23 $mol_{CO}/g_{catalyst}$·h and 2.97 $mol_{CO}/g_{catalyst}$·h (over Pt_1/Fe_2O_3 SAC), and 1.88 $mol_{CO}/g_{catalyst}$·h and 2.12 $mol_{CO}/g_{catalyst}$·h (over Pt_1/CeO_2 SAC), respectively. These results clearly demonstrate that the super activity of CO oxidation on the Pt_1 atoms is also influenced by the reactant gas composition. The nature of the support metal oxide plays an important role as well since the specific rate of Fe_2O_3 supported Pt_1 is different from that of CeO_2 supported Pt_1. When the O_2/CO ratio is close to reaction stoichiometry the difference in reaction rate between the two different metal oxides supports is much smaller.

For CO oxidation at 350 °C, the total activity of the Pt_1/Fe_2O_3 SAC is about 1.5 to 5 times higher that of the nano-Pt/Fe_2O_3 catalyst for different reactant gas compositions (Figure 3) even though the Pt loading of the nano-Pt/Fe_2O_3 catalyst is ~21 times higher than that of the Pt_1/Fe_2O_3 SAC. Moreover, after subtracting the activity contribution from the Fe_2O_3 nanocrystallites the specific reaction rate of the Pt NPs was about 34 to 188 times lower than that of the Pt_1 atoms (Table S1). Similarly, the total activity of the Pt_1/CeO_2 SAC is 1.2 to 4.4 times higher that of the nano-Pt/CeO_2 catalyst (Figure 3) even though the Pt loading of the nano-Pt/CeO_2 catalyst is ~ 42 times higher than that of the Pt_1/CeO_2 SAC. After subtracting the activity contribution from the CeO_2 nanocrystallites, the specific reaction rate of CeO_2 supported Pt NPs is about 49 to 199 times lower than that of the CeO_2 supported Pt_1 atoms (Table S1). From these analyses, one can unambiguously conclude that for CO oxidation at 350°C our as-prepared Pt_1/Fe_2O_3 SAC with a Pt loading of only ~ 30 ppm possesses a performance similar to, or better than, that of the nano-Pt/Fe_2O_3 catalyst with a Pt loading of ~ 1.0 wt.%. For CO oxidation in the temperature range of 260°C-350°C, the 0.03wt% Pt_1/Fe_2O_3 and Pt_1/CeO_2 SAC can be used for practical applications.

For CO oxidation on reducible metal oxide supported metal NP catalysts, the metal atoms located along the perimeters between the metal NPs and the support are often considered as the main active sites.[36-38] If we assume that only the perimeter Pt atoms act as the active centers for CO oxidation over the nano-Pt/Fe_2O_3 and nano-Pt/CeO_2 catalysts, then we can estimate

their TOF values based on the average sizes of the Pt particles. The average sizes of the Pt particles supported on the Fe_2O_3 and CeO_2 (Figure S5 and Figure S6) were measured to be 1.3 ± 0.1 nm and 4.0 ± 0.1 nm, respectively. Therefore, for CO oxidation over the nano-Pt/Fe_2O_3 catalyst the TOFs on the perimeter Pt atoms are estimated to be 28.0, 63.3 and 12.9/s (Figure S9a) with the O_2/CO ratio of 0.5, 1.0 and 4.0, respectively, about 20 to 111 times lower than those on the isolated Pt_1 atoms in the Pt_1/Fe_2O_3 SAC. Similarly, we estimated that the perimeter Pt TOFs in the nano-Pt/CeO_2 catalyst are 12.0, 17.0 and 37.8/s (Figure S9a) with the O_2/CO ratio of 0.5, 1.0 and 4.0, respectively, about 20 to 82 times lower than those of the Pt_1 atoms in the Pt_1/CeO_2 SAC.

The above analyses and discussions unambiguously demonstrate that in comparison to that of the nano-Pt/Fe_2O_3 and nano-Pt/CeO_2 catalysts the Pt_1/Fe_2O_3 and Pt_1/CeO_2 SACs possess super active properties with extremely high TOF values. Our catalytic testing results imply that the Pt_1 atoms are intrinsically much more active than the perimeter atoms of Pt NPs for CO oxidation at elevated temperatures. The experimentally observed high specific reaction rate of the Pt_1/Fe_2O_3 and Pt_1/CeO_2 SACs is originated not only from the 100% dispersion but also from the significantly higher intrinsic activity of each Pt_1 atom, which is further confirmed by the different apparent activation energies as shown in Figure S10.

3. 3 The Unique Behavior of Super Active Pt_1 SAC for CO oxidation

Single-crystal Pd metal has been reported to possess hyperactivity for CO oxidation under ultra-high vacuum conditions and the TOF (CO_2 formation rate) is reported to be as high as 40,000 $site^{-1} \cdot s^{-1}$ at 525 K in 0.5 Torr CO and 9.5 Torr O_2.[39] In order to compare with the UHV single crystal results, a single Pd_1/Fe_2O_3 SAC with a Pd loading of 0.17 wt.% (by ICP-MS) is synthesized. As confirmed by the HAADF-STEM imaging method (Figure S11), the Pd_1 atoms were still in the form of isolated atoms after CO oxidation, which assures that the measured catalytic activity originated from the Pd_1 atoms rather than Pd clusters or NPs. The maximum TOF (32.6/s) on the Pd_1/Fe_2O_3 SAC occurred at 340 ^oC (Figure S12), ~50 times lower than that of the Pt_1/Fe_2O_3 SAC. Furthermore, the TOF decreased to 22.6/s at 350 ^oC, ~63 times lower than that of the Pt_1/Fe_2O_3 SAC. At lower reaction temperatures (40 ^oC to 120 ^oC), the Pd_1/Fe_2O_3 SAC, however, yielded much higher activity than that of the Pt_1/Fe_2O_3 SAC (Figure S13a). When the reaction temperature was >140 ^oC (Figure S13b-c), the catalytic activity of the Pt_1/Fe_2O_3 SAC became higher than that of the Pd_1/Fe_2O_3 SAC and was much higher at reaction temperatures >260 °C. These results indicate that unlike the behavior of the

single-crystal Pd under ultra-high vacuum conditions, the Pd_1/Fe_2O_3 SAC does not show significant super activity behavior for CO oxidation at elevated temperatures. Hence, the super active property of the Pt_1/Fe_2O_3 and Pt_1/CeO_2 SACs may originate from factors that are different from the previously reported hyperactivity of single crystals under UHV conditions.

At elevated temperatures, ignition of CO molecules on Pt single crystal systems has been reported[40-42]. Based on our experimental data for CO oxidation on Fe_2O_3 and CeO_2 supported Pt NPs at high reaction temperatures, it is justifiable to conclude that no super activity behavior would be observable on Pt NPs. Furthermore, Pt_1 atoms on γ-Al_2O_3 did not demonstrate any super activity behavior either. All these results unambiguously show that the observed super activity of Fe_2O_3 and CeO_2 supported Pt_1 is unique to only Pt_1 atoms supported on highly reducible metal oxides such as Fe_2O_3 and CeO_2. Furthermore, as we have discussed earlier, Fe_2O_3 supported Pd_1 atoms did not show the super active behavior for CO oxidation at elevated temperatures. Therefore, the experimentally observed super active property of the Pt_1/Fe_2O_3 and Pt_1/CeO_2 SACs must be related to the intrinsic nature of Pt atoms and how they interact with the support surfaces.

3. 4 Local Coordination and Electronic Structure of Pt_1 SACs

To identify the unique nature of the Pt_1 atoms in the Pt_1/Fe_2O_3 and Pt_1/CeO_2 SACs, X-ray absorption experiments have been conducted to probe the local structure and electronic states of the Pt_1 species. Extended X-ray absorption fine structure spectroscopy (EXAFS) data provided further evidence on the atomic dispersion and local geometric configuration of the Pt species supported on the Fe_2O_3 and CeO_2 powders.[43-45] The EXAFS functions and fitting details of the Pt L_3-edge filtered k^2-weighted $\chi(k)$ obtained on the Pt_1/Fe_2O_3 and Pt_1/CeO_2 SACs have been listed in Table S2. As shown in Figure S14, both the Pt_1/Fe_2O_3 and Pt_1/CeO_2 SACs predominantly exhibit the Pt-O bonds located at approximately 2.0 Å[46], suggesting that the Pt species are mainly in the form of Pt_1 atoms dispersed on the surfaces of Fe_2O_3 and CeO_2 powders, corroborating the conclusion from the STEM imaging results. For the nano-Pt/Fe_2O_3 and nano-Pt/CeO_2 catalysts, they both exhibit weak Pt-O bonds (approximate bond length of 2.0 Å) and relatively strong Pt-Pt bonds (approximate bond length of 2.7 Å). The first shell coordination number (CN), bond length, and the corresponding standard deviations are extracted by curve-fitting based on the two main peaks in the R range of 0-3.0 Å (Table S2). On average, each Pt atom is coordinated with three oxygen atoms (CN = 2.8 for nano-Pt/Fe_2O_3 and CN = 3.0 for nano-Pt/CeO_2), which agrees well with the reported coordination structure of

oxides supported Pt catalysts (CN = 2 & 3) in the public literature.[46-48] On the other hand, each Pt_1 atom in the Pt_1/Fe_2O_3 and Pt_1/CeO_2 SACs is coordinated with four O atoms (CN = 4.4 for Fe_2O_3 supported Pt_1 and CN = 4.0 for CeO_2 supported Pt_1), which indicates that the isolated Pt_1 atoms in the Pt_1/Fe_2O_3 SAC and Pt_1/CeO_2 SAC possess a Pt_1-O_4 configuration. These results suggest that the local coordination environments of the Pt_1 atoms are totally different from those of the small Pt NPs.

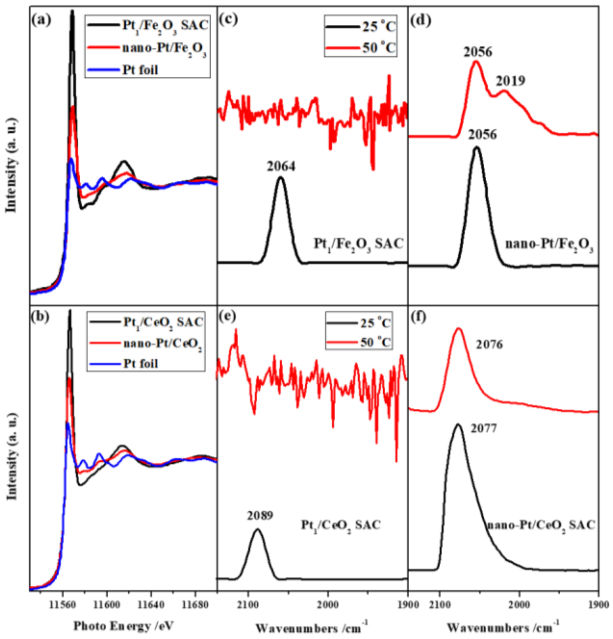

Figure 4 XANES spectra at the Pt L_3-edge of Pt_1 atoms and Pt particles of Pt_1/Fe_2O_3 SAC and nano-Pt/Fe_2O_3 (a) and Pt_1/CeO_2 SAC and nano-Pt/CeO_2 (b); In-situ CO-DRIFTs of Pt_1/Fe_2O_3 SAC (c) and nano-Pt/Fe_2O_3 (d), Pt_1/CeO_2 SAC (e) and nano-Pt/CeO_2 (f) at 25 and 50 °C. The XANES spectra reveal a decreasing trend in the intensity of the Pt L_3 white-line: Pt_1/Fe_2O_3 SAC (2.57) > nano-Pt/Fe_2O_3 (1.70) > Pt foil (1.23) and Pt_1/CeO_2 SAC (2.14) > nano-Pt/CeO_2 (1.63) > Pt foil (1.29). The numbers in the parentheses refer to the normalized absorption height for different samples. The peak intensities of the CO-DRIFTs are normalized.

To unravel the electronic structures of the Pt_1 atoms and Pt NPs supported on the reducible Fe_2O_3 and CeO_2, X-ray absorption near-edge structure (XANES) analysis was conducted. As shown in Figure 4a, the Pt white-line intensity of the Pt_1/Fe_2O_3 SAC and nano-Pt/Fe_2O_3 (11568 eV) is significantly higher than that of the Pt foil, confirming that both the Pt_1 atoms and the small Pt nanoparticles are oxidized, probably via electron transfer from the Pt species to the metal oxide support.[5] Furthermore, the white-line intensity of the Pt_1/Fe_2O_3 SAC is considerably higher than that of the nano-Pt/Fe_2O_3, indicating that the Pt_1 atoms possess much higher oxidation states compared to that of the Pt NPs. These conclusions apply to the Pt_1/CeO_2 SAC and nano-Pt/CeO_2 catalyst as well (Figure 4b).

The peak area of the normalized XANES spectra at the Pt L_3-edge is proportional to the amount of unoccupied Pt 5*d* orbitals.[49, 50] By applying a simplified formula (see details in Table S2), the total amount of unoccupied Pt 5*d* orbitals in both the Pt_1/Fe_2O_3 SAC and Pt_1/CeO_2 SAC is estimated to be ~1.1 times higher than that in the nano-Pt/Fe_2O_3 and nano-Pt/CeO_2 catalysts, respectively, implying that more electrons might have been transferred from the Pt_1 to the metal oxides, leading to a stronger EMSI (electronic metal-support interaction) for Pt_1 SACs.[5, 51] Larger amount of unoccupied Pt 5*d* orbitals enables weakening of the CO adsorption strength since the back-donation interaction between the Pt species and CO molecules is reduced due to the fewer available electrons in the Pt 5*d* orbitals.[52] By using Bade charge analysis, and calibrating with common Pt oxides PtO, Pt_3O_4, PtO_2 as listed in Figure S, we identify the oxidation state of Pt in SCAs close to Pt_3O_4, i.e., $Pt^{2.67+}$, which is in line with the DRIFTs and XANES data.

The in-situ CO-DRIFTS results further corroborate that the CO adsorption strength on Pt atoms is significantly weaker than that on Pt NPs (Figure 2 c-f). The linear CO adsorption species, centered at 2064 cm^{-1} and 2056 cm^{-1} on Pt_1/Fe_2O_3 SAC and nano-Pt/Fe_2O_3 (Figure 4 c-d), respectively, were detected at 25 ^oC. When the sample temperature increased from 25 ^oC to 50 ^oC the CO adsorption species were barely observable on the Pt_1/Fe_2O_3 but they were clearly detected on the nano-Pt/Fe_2O_3. The significant blue-shift of the CO absorption peak indicates that the valance of the Pt_1 atoms is higher than the Pt NPs, in agreement with the XANES results. The in-situ CO-DRIFTS data shows similar conclusion for the Pt_1/CeO_2 and nano-Pt/CeO_2 systems (Figure 4e-f). The DRIFTS results corroborate those of the XANES and Bade charge analysis data that higher amount of unoccupied Pt 5*d* orbitals significantly weakens the CO adsorption strength. The less strongly bonded CO molecules to the Pt_1 atoms facilitate the CO oxidation process, leading to significantly enhanced catalytic activity.[5, 53]

3. 5 Proposed Catalytic Mechanism via DFT Calculations

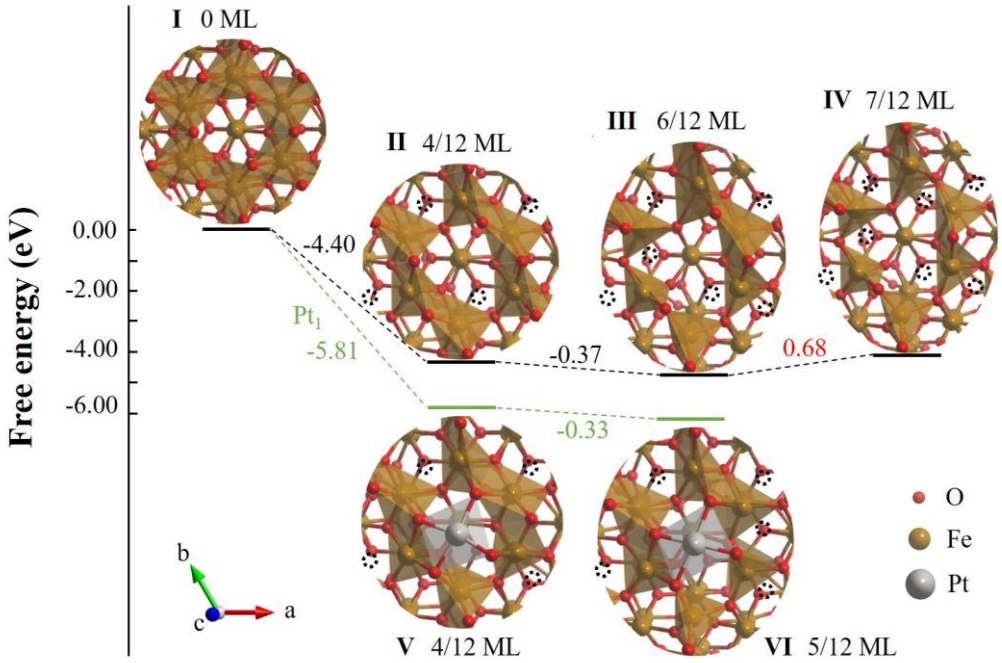

Figure 5 Evolution of Fe_2O_3 (001) surface under synthesis condition (300 ºC in air, 0.05 MPa O_2 partial pressure). The dotted black circles represent surface oxygen vacancies, and its coverage is in the unit of monolayer (ML). The calculated free energies are referenced to gas phase O_2 and bulk Pt.

To uncover the fundamental mechanism that governs the ultra-high activity and stability of the Pt_1/Fe_2O_3 and Pt_1/CeO_2 SACs, we take Pt_1/Fe_2O_3 SAC as a representative example to explore the potential catalytic mechanisms on these two catalysts via density functional theory (DFT) calculations. We firstly performed DFT calculations on the synthesis processes. The local coordination environment of the atomically dispersed Pt atoms on the Fe_2O_3 (001) surface underpins the catalytic activity and stability, therefore, appropriate physical model of the as prepared SACs is critical. Figure 5 shows the detailed structural evolution of the Fe_2O_3 (001) surface with and without the presence of Pt_1 atom. The modelling of structure evolution starts from an oxygen-rich (001) surface (step I), a hexagonal surface geometry comprising six edge-shared FeO_6 octahedra. One third of the topmost surface oxygen of the FeO_6 unit could easily desorb to form a six edge-shared FeO_5 square pyramid and 1/3 monolayer (ML) surface oxygen vacancies (step II). This process is extremely exothermic (-4.40 eV) under synthesis condition, which can even take place at room temperature. Without Pt atom loading, the surface will be

stabilized in 1/2 ML surface oxygen vacancies (step III) with the removal of another two oxygen, resulting in a squeezed hexagonal geometry comprising four point-shared tetrahedra, and two edge-shared square pyramids. While Pt_1 atom can stabilize the surface at 5/12 ML surface oxygen vacancies with the formation of Pt_1-O_4 square planar (step VI), which agrees well with our EXAFS data. The binding energy of the Pt_1 is about -1.41 eV, against Pt agglomeration into bulk at high temperatures.

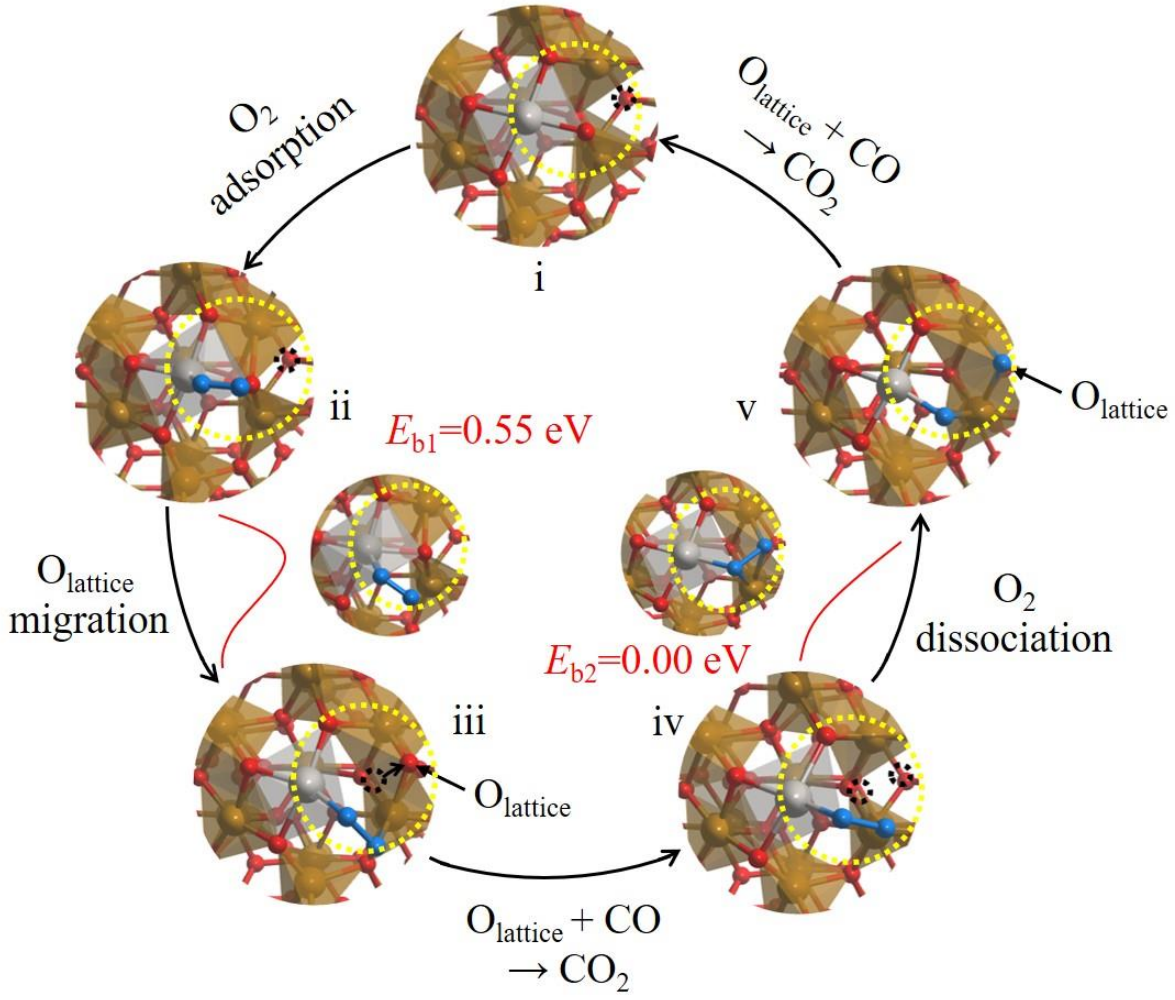

Figure 6 Non-classical MvK CO oxidation mechanism with lattice oxygen migration and activation under gas-phase O_2 adsorption on four-fold coordinated single Pt atoms. *The blue balls represent adsorbed oxygen. The active region has been highlighted by bright yellow circles.*

The four-oxygen coordination of Pt_1-O_4 yields a high-valence Pt site as confirmed by the XANES and CO-DRIFTs measurements. DFT results show that both O_2 and CO molecules can be adsorbed on the high-valence Pt site with around -0.5 eV and -0.8 eV binding energies, respectively. These adsorption energies are relatively weak comparing to that on the Pt surface,

avoiding CO poisoning on the Pt_1 atom, but also leading to the difficulty in O_2 activation because of the deep Pt 5*d* band of Pt_1-O_4. Indeed, that is the reason why high-valence Pt sites are not considered catalytically active for CO oxidation.[54] However, it is found that an unusual catalytic mechanism exists to change the catalytic behavior of our stable Pt SACs. Figure 6 displays a non-classical MvK catalytic cycle for CO oxidation on the Pt_1/Fe_2O_3. Although the four-oxygen coordinated Pt_1 atom cannot directly activate O_2, the adsorbed O_2, however, facilitates the movement of the coordination oxygen atoms with a small barrier (0.55 eV). Upon O_2 adsorption, one of the coordination oxygen atoms can facilely break the Pt-O bond and migrates into a nearby surface oxygen vacancy site. Meanwhile, the adsorbed end-on O_2 will bridge the Pt and Fe site by forming a Pt-OO-Fe configuration (step ii to iii). The migrated coordination oxygen atom can then directly combine with the adsorbed CO to form a CO_2 molecule which readily desorbs, recovering the oxygen vacancy site (step iv). The subsequent O_2 dissociation process becomes barrierless through O_2 adsorption on the Pt-Fe_2 triangle (step iv to v), which can dissociate the O_2 molecule with zero activation energy. The side-view images of O_2 adsorption configurations are presented in Figure S16 to better demonstrate the process of O_2 activation. Thereafter, one of the split oxygen atoms replenishes the consumed coordination oxygen in the Pt_1-O_4 configuration, while the other one fills into the nearby surface oxygen vacancy again and can directly oxidize CO into CO_2 to recover the initial catalyst surface (step i). Overall, the CO oxidation can be efficiently catalyzed by the high-valence Pt site with four oxygen coordination through a non-classical MvK reaction pathway, indicating a promising design strategy for stable and active SACs. The detailed change on free energy (ΔG) of each elementary step during CO oxidation by non-classic MvK mechanism has been listed in Table S3.

3. 6 Potential Practical Applications of Super Active Pt_1 SACs

Platinum plays a crucial role in the three-way catalysts (TWCs) that have been widely used in automobiles for emission control, primarily due to its excellent oxidation and reduction ability in the removal of CO[55, 56], hydrocarbons (HCs) [57] and NO_x [58-60]. However, the expensive Pt with limited resources will not be sustainable. Therefore, development of abundant alternatives or to significantly minimize the usage of Pt becomes crucial.[61] The work reported in this paper clearly demonstrates that by using atomically dispersed Pt atoms the Pt specific reaction rates of the Pt_1/Fe_2O_3 and Pt_1/CeO_2 SACs are more than 2 orders of magnitude higher than that of commercial TWCs (0.5 wt.% Pt/γ-Al_2O_3 and 0.5 wt.%

$Pt/CeO_2/\gamma\text{-}Al_2O_3$) for CO oxidation at 350 ^oC (Table S1).[62] The total catalytic activity (calculated based on the total catalyst weight that includes both the noble metal and the oxide support) of the synthesized Pt_1/CeO_2 and Pt_1/Fe_2O_3 SACs is more than 185 and 452 times higher than that of the commercial 0.5 wt.% $Pt/CeO_2/\gamma\text{-}Al_2O_3$ at 350 ^oC. Therefore, the super active Pt_1-based SACs may be an excellent candidate to replace the Pt NPs in the TWCs, leading to the significant reduction of the usage of the costly Pt. The practical applications of such extremely low levels (10-50 ppm) of Pt to emission controls may have major societal impact and significantly enhance the sustainability of rare and expensive resources.

4. Conclusions

We have reported the unique super activity behavior for high temperature CO oxidation on extremely low Pt loading and stable Pt_1/Fe_2O_3 and Pt_1/CeO_2 SACs. The total activity of the as-synthesized Pt_1/Fe_2O_3 SAC with a Pt loading of only ~30 ppm is comparable to that of the .0 wt.% nano-Pt/Fe_2O_3 for CO oxidation at 350 ^oC. DFT calculations reveal that the Pt_1-O_4 configuration not only catalyzes CO oxidation through a non-classical MvK reaction pathway but also stabilizes the Pt_1 atoms. The super active and stable Pt_1/Fe_2O_3 and Pt_1/CeO_2 SACs may become a potential candidate to replace the Pt NPs that are used in the current commercial TWCs, leading to significant reduction in cost and sustainable use of expensive and rare resources. Although this work only explored the super activity nature of Pt_1/Fe_2O_3 and Pt_1/CeO_2 SACs it is expected that other types of metal and support combinations may provide similar behavior. The discovery of super active and stable SACs that operate at elevated reaction temperatures provides an alternative route to practical applications of SACs that can significantly reduce the cost of goods.

Conflict of Interest

The authors declare that they have no known competing financial interests or personal relationships that could have appeared to influence the work reported in this paper.

Supporting Information

STEM images, X-ray Absorption data, electronic and chemical properties data, catalytic activity data and DFT calculation data.

AUTHOR INFORMATION

Corresponding Author

E-mail: yang.lou@jiangnan.edu.cn; yp.zheng@siat.ac.cn; jingyue.liu@asu.edu.

Author Contributions

The manuscript was written through contributions of all authors. All authors have given approval to the final version of the manuscript. Y. L. synthesized the catalysts, designed and tested the experiments, analyzed the data, drafted and revised the manuscript. W. G. assisted to synthesize catalysts and test the experiments. Y.Z. conducted the DFT work and revised the manuscript. J. L. conducted the STEM work, discussed the results and revised the manuscript.

Funding Sources

This work is supported by the National Natural Science Foundation of China (21908079 and 51902339), the National Science Foundation under Grant No. 1465057 (CHE-1465057) and 1955474 (CHE-1955474), and Startup Funding at Jiangnan University (1045210322190170).

Acknowledgement

The authors gratefully acknowledge the use of facilities within the Eyring Materials Center and the John M. Cowley Center for High Resolution Electron Microscopy at Arizona State University. The authors gratefully acknowledge Dr. Tao Li, Dr. Chengjun Sun and Dr. Gang Wan for collecting and analyzing the XAS data by using the resources of the Advanced Photon Source, an Office of Science User Facility operated for the U. S. Department of Energy (DOE) Office of Science by Argonne National Laboratory. YL acknowledges Dr. Qiguang Dai (East China University of Science and Technology) and Prof. Dong Yang (Nanjing Tech University) for helpful discussions. One official patent application of this work has been filed to United States Patent and Trademark Office application (application number: 16/898,173) after we filed one provisional patent application (application number: 62/860,084).

REFERENCES

1 Y. Lou, J. Ma, W.D. Hu, Q. G. Dai, L. Wang, W. C. Zhan, Y. L. Guo, X. M. Cao, Y. Guo, P. Hu, G. Z. Lu, Low-temperature methane combustion over Pd/H-ZSM-5: active Pd sites with specific electronic properties modulated by acidic sites of H-ZSM-5, *ACS Catal.* **2016**, 6 (12), 8127-8139.

2 N. M. Schweitzer, J. A. Schaidle, O. K. Ezekoye, X. Pan, S. Linic, L. T. Thompson, High activity carbide supported catalysts for water gas shift, *J. Am. Chem. Soc.* **2011**, 133, 2378-2381.

3 G. F. Zhou, J. Ma, S. Bai, L. Wang, Y. Guo, CO catalytic oxidation over Pd/CeO_2 with different chemical states of Pd, *Rare Metals.* **2019**, 39, 800-805.

4 A. Wang, J. Li, T. Zhang, Heterogeneous single-atom catalysis, *Nat. Rev. Chem.* **2018**, 2 (6), 65-81.

5 B. Qiao, A. Wang, X. Yang, L. F. Allard, Z. Jiang, Y. Cui, J. Liu, J. Li, T. Zhang, Single-atom catalysis of CO oxidation using Pt_1/FeO_x, *Nat. Chem.* **2011**, 3 (8), 634-641.

6 L. Liu, A. Corma, Metal catalysts for heterogeneous catalysis: from single atoms to nanoclusters and nanoparticles, *Chem. Rev.* **2018**, 118 (10), 4981-5079.

7 Z. X. Wei, Y. T. Zhu, J. Y. Liu, Z. C. Zhang, W. P. Hu, H. Xu, Y. Z. Feng, J. M. Ma, Recent advance in single-atom catalysis, *Rare Metals*. **2021**, 40, 767-789.

8 Y. Lou, F. jiang, W. Zhu, L. Wang, T. Yao, S. Wang, B. Yang, B. Yang, Y. Zhu, X. Liu, CeO_2 supported Pd dimers boosting CO_2 hydrogenation to ethanol, *Applied Catalysis B: Environmental*. **2021**, 291, 120122.

9 L. Fan, P. F. Liu, X. Yan, L. Gu, Z. Z. Yang, H. G. Yang, S. Qiu, X. Yao, Atomically isolated nickel species anchored on graphitized carbon for efficient hydrogen evolution electrocatalysis, *Nat. Commun.* **2016**, 7, 10667.

10 G. Gao, Y. Jiao, E. R. Waclawik, A. Du, Single atom (Pd/Pt) supported on graphitic carbon nitride as an efficient photocatalyst for visible-light reduction of carbon dioxide, *J. Am. Chem. Soc.* **2016**, 138 (19), 6292-6297.

11 J. Jones, H. F. Xiong, A. T. Delariva, E. J. Peterson, H. Pham, S. R. Challa, G. S. Qi, S. Oh, M. H. Wiebenga, X. I. P. Hernandez, Y. Wang, A. K. Datye, Thermally stable single-atom platinum-on-ceria catalysts via atom trapping, *Science* **2016**, 353 (6295), 150-154.

12 Y. Lou, J. Xu, Y. Zhang, C. Pan, Y. Dong, Y. Zhu, Metal-support interaction for heterogeneous catalysis: from nanoparticles to single atoms, *Mater. Today Nano* **2020**, 12 100093.

13 Y. Lou, Y. Cai, W. Hu, L. Wang, Q. Dai, W. Zhan, Y. Guo, P. Hu, X. M. Cao, J. Liu, Y. Guo,

Identification of active area as active center for CO oxidation over single Au atom catalyst, *ACS Catal.* **2020**, 10, 6094-6101.

14 Y. Lou, Y. Zheng, X. Li, N. Ta, J. Xu, Y. Nie, K. Cho, J. Liu, Pocketlike active site of Rh_1/MoS_2 single-atom catalyst for selective crotonaldehyde hydrogenation, *J. Am. Chem. Soc.* **2019**, 141, 19289-19295.

15 L. Zhang, Y. Ren, W. Liu, A. Wang, T. Zhang, Single-atom catalyst: a rising star for green synthesis of fine chemicals, *Natl. Sci. Rev.* **2018**, 5, 653-672.

16 Y. Chen, S. Ji, C. Chen, Q. Peng, D. Wang, Y. Li, Single-atom catalysts: synthetic strategies and electrochemical applications, *Joule* **2018**, 2, 1242-1264.

17 X. Tang, L. Wang, B. Yang, C. Fei, T. Yao, W. Liu, Y. Lou, Q. Dai, Y. Cai, X.-M. Cao, W. Zhan, Y. Guo, X.-Q. Gong, Y. Guo, Direct oxidation of methane to oxygenates on supported single Cu atom catalyst, *Appl. Catal. B: Environ.* **2021**, 285, 119827.

18 X. Zhao, Y. G. Li, Two-electron oxygen reduction reaction by high-loading molybdenum single-atom catalysts, *Rare Metals*. **2021**, 39, 455-457.

19 R. Kumar, M. Kumar, Single-atom catalysts boosted ultrathin film sensors, *Rare Metals*. **2020**, 39, 1110-1112.

20 H. Yan, H. Cheng, H. Yi, Y. Lin, T. Yao, C. Wang, J. Li, S. Wei, J. Lu, Single-atom Pd_1/graphene catalyst achieved by atomic layer deposition: remarkable performance in selective hydrogenation of 1, 3-butadiene, *J. Am. Chem. Soc.* **2015,** 137, 10484-10487.

21 M. Moses-DeBusk, M. Yoon, L. F. Allard, D. R. Mullins, Z. Wu, X. Yang, G. Veith, G. M. Stocks, C. K. Narula, CO oxidation on supported single Pt atoms: experimental and ab initio density functional studies of CO interaction with Pt atom on theta-Al_2O_3 (010) surface, *J. Am. Chem. Soc.* **2013**, 135, 12634-12645.

22 G. S. Parkinson, Z. Novotny, G. Argentero, M. Schmid, J. Pavelec, R. Kosak, P. Blaha, U. Diebold, Carbon monoxide-induced adatom sintering in a Pd-Fe_3O_4 model catalyst, *Nat. Mater.* **2013**, 12, 724-728.

23 P. X. Liu, Y. Zhao, R. X. Qin, S. G. Mo, G. X. Chen, L. Gu, D. M. Chevrier, P. Zhang, Q. Guo, D. D. Zang, B. H. Wu, G. Fu, N. F. Zheng, Photochemical route for synthesizing atomically dispersed palladium catalysts, *Science* **2016**, 352, 797-801.

24 F. Schüth, Colloidal deposition as method to study the influence of the support on the activity of gold catalysts in CO-oxidation, *Phys. Status Solidi B* 2013, 250, 1142-1151.

25 E. H. K. Ziegler, H. Breil, H. Martin, Das Mülheimer Normaldruck-Polyäthylen-Verfahren, *Angew. Chem. Int. Ed.* **1955**, 67, 541-547.

26 P. P. G. Natta, P. Corradini, F. Danusso, E. Mantica, G. Mazzanti, G. Moraglio, Crystalline

high polymers of α-olefins, *J. Am. Chem. Soc.* **1955**, 77, 1708-1710.

27 T. T. N. Kashiwa, H. Fujimura, US Patent, 3, 642, 746, USA, 1967.

28 K. S. Thushara, R. Mathew, T. G. Ajithkumar, P. R. Rajamohanan, S. Bhaduri, C. S. Gopinath, $MgCl_2 \cdot 4(CH_3)_2CHOH$: a new molecular adduct and super active polymerization catalyst support, *J. Phys. Chem.* C **2009**, 113, 8556-8559.

29 H. Makio, N. Kashiwa, T. Fujita, FI catalysts: A new family of high sperformance catalysts for olefin polymerization, *Adv. Synth. Catal.* **2002**, 344, 477-493.

30 X. K. Gu, B. Qiao, C. Q. Huang, W.-C. Ding, K. Sun, E. Zhan, T. Zhang, J. Liu, W.-X. Li, Supported single Pt_1/Au_1 atoms for methanol steam reforming, *ACS Catal.* 2014, 4, 3886-3890.

31 N. Ashburn, Y. Zheng, S. Thampy, S. Dillon, Y. J. Chabal, J. W. P. Hsu, K. Cho, Integrated experimental-theoretical approach to determine reliable molecular reaction mechanisms on transition-metal oxide surfaces, *ACS Appl. Mater. Interfaces* **2019**, 11, 30460-30469.

32 G. Kresse, J. Furthmüller, Efficiency of ab-initio total energy calculations for metals and semiconductors using a plane-wave basis set, *Comput. Mater. Sci.* **1996**, 6, 15-50.

33 P. E. Blochl, Projector augmented-wave method, *Phys. Rev. B Condens. Matter.* **1994**, 50, 17953-17979.

34 J. P. Perdew, K. Burke, M. Ernzerhof, Generalized gradient approximation made simple, *Phys. Rev. Lett.* **1996**, 77, 3865-3868.

35 S. Y. Li, G. Liu, H. L. Lian, M. J. Jia, G. M. Zhao, D. Z. Jiang, W. X. Zhang, Low-temperature CO oxidation over supported Pt catalysts prepared by colloid-deposition method, *Catal. Commun.* **2008**, 9, 1045-1049.

36 M. Cargnello, V.V. Doan-Nguyen, T.R. Gordon, R.E. Diaz, E.A. Stach, R.J. Gorte, P. Fornasiero, C. B. Murray, Control of metal nanocrystal size reveals metal-support interface role for ceria catalysts, *Science* **2013**, 341, 771-773.

37 I. X. Green, W. Tang, M. Neurock, J. T. Yates, Spectroscopic observation of dual catalytic sites during oxidation of CO on a Au/TiO_2 catalyst, *Science* **2011**, 333, 736-739.

38 M. Date, M. Okumura, S. Tsubota, M. Haruta, Vital role of moisture in the catalytic activity of supported gold nanoparticles, *Angew. Chem. Int. Ed.* **2004**, 43, 2129-2132.

39 M. S. Chen, Y. Cal, Z. Yan, K. K. Gath, S. Axnanda, D. W. Goodman, Highly active surfaces for CO oxidation on Rh, Pd, and Pt, *Surf. Sci.* **2007**, 601, 5326-5331.

40 X. C. Su, P. S. Cremer, Y. R. Shen, G. A. Somorjai, High-pressure CO oxidation on Pt (111) monitored with infrared-visible sum frequency generation (SFG), *J. Am. Chem. Soc.* **1997**, 119, 3994-4000.

41 K. R. McCrea, J. S. Parker, G. A. Somorjai, The role of carbon deposition from CO

dissociation on platinum crystal surfaces during catalytic CO oxidation: Effects on turnover rate, ignition temperature, and vibrational spectra, *J. Phys. Chem. B* **2002**, 106, 10854-10863.

42 S. H. Joo, J. Y. Park, C. K. Tsung, Y. Yamada, P. Yang, G. A. Somorjai, Thermally stable Pt/mesoporous silica core-shell nanocatalysts for high-temperature reactions, *Nat. Mater.* **2009**, 8, 126-131.

43 H. Xu, D. Rebollar, H. He, L. Chong, Y. Liu, C. Liu, C. J. Sun, T. Li, J.V. Muntean, R.E. Winans, D.-J. Liu, T. Xu, Highly selective electrocatalytic CO_2 reduction to ethanol by metallic clusters dynamically formed from atomically dispersed copper, *Nat. Energy* **2020**, 5, 623-632.

44 Z. Liu, Y. Zhong, I. Shafei, S. Jeong, L. Wang, H. T. Nguyen, C. J. Sun, T. Li, J. Chen, L. Chen, Y. Losovyj, X. Gao, W. Ma, X. Ye, Broadband tunable mid-infrared plasmon resonances in cadmium oxide nanocrystals induced by size-dependent nonstoichiometry, *Nano Lett.* **2020**, 20, 2821-2828.

45 G. Ding, L. Hao, H. Xu, L. Wang, J. Chen, T. Li, X. Tu, Q. Zhang, Atomically dispersed palladium catalyses Suzuki-Miyaura reactions under phosphine-free conditions, *Commun. Chem.* **2020**, 3, 43.

46 B. Zhang, H. Asakura, J. Zhang, J. Zhang, S. De, N. Yan, Stabilizing a platinum single-Atom catalyst on supported phosphomolybdic acid without compromising hydrogenation activity, *Angew. Chem. Int. Ed.* **2016**, 55, 8319-8323.

47 J. D. Kistler, N. Chotigkrai, P. Xu, B. Enderle, P. Praserthdam, C. Y. Chen, N. D. Browning, B. C. Gates, A single-site platinum CO oxidation catalyst in zeolite KLTL: microscopic and spectroscopic determination of the locations of the platinum atoms, *Angew. Chem. Int. Ed.* **2014**, 53, 8904-8907.

48 Y. Ren, Y. Tang, L. Zhang, X. Liu, L. Li, S. Miao, D. Sheng Su, A. Wang, J. Li, T. Zhang, Unraveling the coordination structure-performance relationship in Pt_1/Fe_2O_3 single-atom catalyst, *Nat. Commun.* **2019**, 10, 4500.

49 S. Mukerjee, S. Srinivasan, M.P. Soriaga, J. McBreen, Effect of Preparation Conditions of Pt Alloys on Their Electronic, Structural, and Electrocatalytic Activities for Oxygen Reduction - XRD, XAS, and Electrochemical Studies, *J. Phys. Chem.* **1995**, 99, 4577-4589.

50 A. N. Mansour, J. W. Cook, D. E. Sayers, Quantitative technique for the determination of the number of unoccupied d-electron states in a platinum catalyst using the L2, 3 x-ray absorption edge spectra, *J. Phys. Chem.* **1984**, 88, 2330-2334.

51 P. Hu, Z. Huang, Z. Amghouz, M. Makkee, F. Xu, F. Kapteijn, A. Dikhtiarenko, Y. Chen, X. Gu, X. Tang, Electronic metal-support interactions in single-atom catalysts, *Angew. Chem. Int. Ed.* **2014**, 53, 3418-3421.

52 G. Bistoni, S. Rampino, N. Scafuri, G. Ciancaleoni, D. Zuccaccia, L. Belpassi, F. Tarantelli, How π back-donation quantitatively controls the CO stretching response in classical and non-classical metal carbonyl complexes, *Chem. Sci.* **2016**, 7, 1174-1184.

53 Y. Lou, X. M. Cao, J. Lan, L. Wang, Q. Dai, Y. Guo, J. Ma, Z. Zhao, Y. Guo, P. Hu, G. Lu, Ultralow-temperature CO oxidation on an In_2O_3-Co_3O_4 catalyst: a strategy to tune CO adsorption strength and oxygen activation simultaneously, *Chem. Commun. 2014*, 50, 6835-6838.

54 J. Ke, W. Zhu, Y. Jiang, R. Si, Y. J. Wang, S. C. Li, C. Jin, H. Liu, W. G. Song, C. H. Yan, Y. W. Zhang, Strong local coordination structure effects on subnanometer PtO_x clusters over CeO_2 nanowires probed by low-temperature CO oxidation, *ACS Catal.* **2015**, 5, 5164-5173.

55 P. Carlsson, M. Skoglundh, P. Thormählen, B. Andersson, Low-temperature CO oxidation over a Pt/Al_2O_3 monolith catalyst investigated by step-response experiments and simulations, *Top. Catal.* **2004**, 30/31, 375-381.

56 N. An, X. Yuan, B. Pan, Q. Li, S. Li, W. Zhang, Design of a highly active Pt/Al_2O_3 catalyst for low-temperature CO oxidation, *RSC Adv.* **2014**, 4, 38250.

57 J. A. Enterkin, W. Setthapun, J. W. Elam, S. T. Christensen, F. A. Rabuffetti, L. D. Marks, P. C. Stair, K. R. Poeppelmeier, C. L. Marshall, Propane Oxidation over Pt/$SrTiO_3$ Nanocuboids, *ACS Catal.* **2011**, 1, 629-635.

58 C. H. Kim, G. Qi, K. Dahlberg, W. Li, Strontium-doped perovskites rival platinum catalysts for treating NOx in simulated diesel exhaust, *Science* **2010**, 327, 1624-1627.

59 J. Després, M. Elsener, M. Koebel, O. Kröcher, B. Schnyder, A. Wokaun, Catalytic oxidation of nitrogen monoxide over Pt/SiO_2, *Appl. Catal. B: Environ.* **2004**, 50, 73-82.

60 Y. Zhang, Y.B. Yu, H. He, Oxygen vacancies on nanosized ceria govern the NO_x storage capacity of NSR catalysts, *Catal. Sci. Technol.* **2016**, 6, 3950-3962.

61 J. Cooper, J. Beecham, A study of platinum group metals in three-way autocatalysts effect of rhodium loading outweighs that of platinum or palladium, *Platin. Met. Rev.* **2013**, 57, 281-288.

62 A. Papavasiliou, A. Tsetsekou, V. Matsouka, M. Konsolakis, I. V. Yentekakis, An investigation of the role of Zr and La dopants into $Ce_{1-x-y}Zr_xLa_yO_\delta$ enriched γ-Al_2O_3 TWC washcoats, *Appl. Catal. A: Gen.* **2010**, 382, 73-84.